Surfaces and Interfaces 72 (2025) 107127

Contents lists available at ScienceDirect

Surfaces and Interfaces

journal homepage: www.sciencedirect.com/journal/surfaces-and-interfaces

Funnel mechanism for the filtration of gases through nanopores in layered membranes of carbon materials

Sahar Mahnaee [a], María J. López [a,*], Julio A. Alonso [a,b]

[a] Departamento de Física Teórica, Atómica y Óptica, Universidad de Valladolid, 47011 Valladolid, Spain
[b] Donostia International Physics Center (DIPC), 20018 San Sebastián, Spain

ARTICLE INFO

Keywords:
Nanopores
Filtration
Molecular gases
Graphdiyne
Boron graphdiyne

ABSTRACT

Ab initio molecular dynamics simulations provide novel information on the mechanisms of filtration of CO_2 and CH_4 gases through the nanopores of graphdiyne (GDY) and boron-graphdiyne (BGDY) layered materials. The molecules follow a funnel mechanism, in which molecules falling in the catchment area of the funnel (the wide upper region) deviate from their original path and cross the pore through a region around the center of the pore (the narrow tube at the bottom of the funnel). The critical parameter for a successful crossing is the size ratio of molecule and pore. The relevant pore size is not its geometrical size but an effective size accounting for the extension of the electronic cloud of the carbon chains bounding the pore. Very important is also the anisotropy in the form of the molecule. The linear CO_2 molecule can take advantage of the orientation of its axis to decrease the effective size when crossing the narrow pores of GDY. The simulations reveal the relevance of the vibrational motion of the molecules, because the vibrations modulate the effective dynamical size of the molecules.

1. Introduction

In recent years, the necessity of addressing climate change and the increasing awareness of its global impact have spurred a significant amount of research into efficient carbon dioxide (CO_2) separation technologies [1]. One of the most pressing environmental challenges is reducing CO_2 emissions, a major contributor to greenhouse gases. Separating CO_2 from industrial emissions has become a focal point, particularly in sectors where CO_2 is a byproduct of natural gas refinement. Given the environmental and economic pressures, there is an ongoing demand for innovative and effective CO_2 separation techniques [2]. In the gas and petrochemical industries, natural gas is predominantly composed of methane (CH_4), with CO_2 present as an impurity that can negatively impact both the calorific value of the gas and the durability of the processing equipment. Because of its corrosive nature, CO_2 poses potential risks to infrastructure, necessitating its removal to maintain equipment integrity. Therefore, the removal of CO_2 from CH_4 is not only an environmental imperative but also an industrial necessity to enhance the quality and usability of natural gas [3]. Traditional gas separation techniques, including cryogenic distillation and surface adsorption with the help of chemical solvents and physical filters, although effective, have limitations because of energy consumption and operational costs, as well as environmental problems [4].

Meanwhile, carbon-based membranes have been proposed as a promising method for the separation of gas mixtures due to their unique structural and chemical characteristics [5–9]. Some layered carbon materials derived from graphene could be used to design advanced membranes, and structures such as graphdiyne (GDY) [10,11] and boron-graphdiyne (BGDY) [12], which have high chemical stability, have been investigated recently. These and similar materials have layered structures made of pristine or doped carbon chains forming nanometric pores whose size can be controlled by the length of the carbon chains. In this way, the materials offer the possibility of passage or blocking of different molecules selectively [13,14]. In particular, GDY and other graphynes have been investigated for the separation of gases like hydrogen, helium or CO_2 from other components in some gas mixtures [15–24].

These materials, offering the possibility to adjust the pore size and surface chemistry, are apt to make membranes suitable for the separation of CO_2 and CH_4 [14,25]. The difference in the properties of the CO_2 and CH_4 molecules, especially the difference in their shape, can have a significant effect on the separation process. CO_2 is a linear molecule, and CH_4, with four H atoms in tetrahedral configuration around the central C atom, is not far from spherical, so only CO_2 can reorient the molecular

* Corresponding author.
E-mail addresses: sahar.mahnaee@uva.es (S. Mahnaee), mariajlopez@uva.es (M.J. López), jaalonso@uva.es (J.A. Alonso).

https://doi.org/10.1016/j.surfin.2025.107127
Received 24 February 2025; Received in revised form 22 June 2025; Accepted 3 July 2025
Available online 4 July 2025

axis to facilitate the filtration through the pores. This can contribute to the selective separation, as we have found in a previous computational investigation based on density functional theory [25].

However, the gas separation process at the nanoscale is a complex phenomenon that depends on various factors such as the size and shape of the pores, the operating temperature and pressure, and the interaction between molecules and membranes. In order to gain a deeper understanding of the mechanisms involved in this process, molecular dynamics (MD) simulations [26,27] provide a powerful tool to analyze the dynamical behavior of the molecules at the nanoscale. MD simulations give detailed information on the motion and the path of the molecules, the interaction between the molecules and the membrane layers and the dynamics of the processes that lead to crossing or bouncing back of the molecules, thus improving our knowledge of the fundamental mechanisms of separation of gas mixtures [28,29]. Molecular dynamics simulations help to understand how the molecules behave near the membrane and whether they are able to pass through the membrane.

Besides MD simulations, other methods such as density functional theory (DFT) and Monte Carlo have also been used. Each of these methods brings specific features that are useful for investigating different aspects of the filtration through membranes. DFT is capable of looking at the electronic properties and the interaction forces, and MD simulations are suitable for analyzing the dynamical behavior. Combining these methods, that is, using a DFT-MD formalism, in which the interactions are self-consistently calculated *on the fly*, can achieve accurate results that can help in the design of efficient gas separation membranes [30].

Based on the simulation results, membranes having pores with appropriate size can improve the separation of CO_2 from CH_4. Using that information to optimize parameters such as the membrane thickness, the amount and shape of pores, and the internal structure of the membranes, can be useful in developing a new generation of high-performance carbon membranes [31]. This can help to design membranes with optimal structures and high operational potential which can show good efficiency on an industrial scale.

In this study, the process of passage of CO_2 and CH_4 gases through specific carbon-derived layered porous membranes, such as GDY and BGDY, has been investigated using DFT-MD simulations. The simulations allow for a fundamental analysis of the interaction between gases and membranes, and allow to understand the processes of filtering through the membranes. We have discovered that the passage through the nanopores of the membranes can benefit from a *funnel* mechanism. These results enhance our understanding of the permeation process, and open new horizons in the field of gas separation technologies using carbon membranes.

2. Computational method

The passage or retention of the CO_2 and CH_4 molecules through the nanometric pores of GDY and BGDY single layer membranes has been investigated by performing ab initio molecular dynamics simulations (AIMD). At every time step of the dynamical simulations, the electronic structure, energy and forces on the atoms of the molecule-membrane system are calculated by solving the Kohn-Sham (K-S) equations of DFT [32] as implemented in the Quantum Espresso (QE) suite of codes [33,34]. The spin polarized version of DFT has been used. The interactions between the valence electrons and the ionic cores are modeled by projector augmented wave (PAW) pseudopotentials [35]. One, two, four, and six valence electrons are taken into account for the hydrogen, boron, carbon, and oxygen atoms, respectively [36]. The generalized gradient approximation of Perdew, Burke and Ernzerhof (GGA-PBE) [37] is used for the exchange-correlation functional, and dispersion interactions are considered at the Grimme's DFT-D3 [38] level. A plane-wave basis set is employed for the expansion of the K-S orbitals and of the electron density, with energy cutoffs of 45 Ry and 350 Ry, respectively, and a Monkhorst-Pack [39] grid of $2 \times 2 \times 1$ k-points is used to sample the Brillouin zone of the reciprocal lattice.

The structure of the GDY membrane is shown in Fig. 1. Carbon hexagons are linked by diacetylenic chains and form a planar layer having triangular pores [40]. On the other hand, BGDY has the structure of a planar hexagonal honeycomb layer, with boron atoms on the vertices of the hexagons. The B atoms are linked by diacetylenic carbon chains. Both membranes, GDY and BGDY, are modelled using the supercell methodology, with periodic boundary conditions. Thus, the GDY layer is modelled by a trigonal supercell, with in-plane cell parameter of length $a = 18.8986$ Å, containing 72 C atoms. The BGDY layer is modelled also by a trigonal supercell with in-plane cell parameter $a = 23.6772$ Å, containing 48 C atoms and 8 B atoms. In both cases, the cell parameter in the direction perpendicular to the layer is taken sufficiently large, 14 Å, so that the interaction between layers in different cells can be neglected.

Constant energy MD simulations have been performed for the molecules moving towards the membrane using the Verlet algorithm as implemented in QE suite. At the beginning of the simulation, the structure of the membrane (GDY or BGDY) corresponds to its ground state configuration at temperature $T = 0$ K. Notice that this is only the initial substrate temperature, since we perform constant energy simulations. The molecule (CO_2 or CH_4) is stretched, following the vibrational normal modes, to the maximum amplitude corresponding to the zero-point energy (ZPE) of the molecule: 0.311 eV for CO_2 and 1.175 eV for CH_4. The molecules are initially placed at different positions above the layer at a vertical distance from the membrane of 4 Å (except in special cases to be indicated below, in which, for convenience, the vertical distance was larger than 4 Å). The molecules were then sent towards the layer in the vertical direction at several translational velocities (to be specified below). Due to the mass difference between CO_2 and CH_4, equal initial velocities of the two molecules correspond to different translational kinetic energies. Comparisons between the passage behavior across the membranes of the two molecules are presented for: i) the same incident translational velocity, and ii) the same initial translational kinetic energy.

To assess the effect of the temperature of the membrane on the crossing of molecules across the pores, simulations have also been performed with the layer at initial temperature of 300 K. The isolated layer is first thermalized at 300 K by performing constant temperature simulations using the Andersen thermostat [41]. Then, the coordinates and

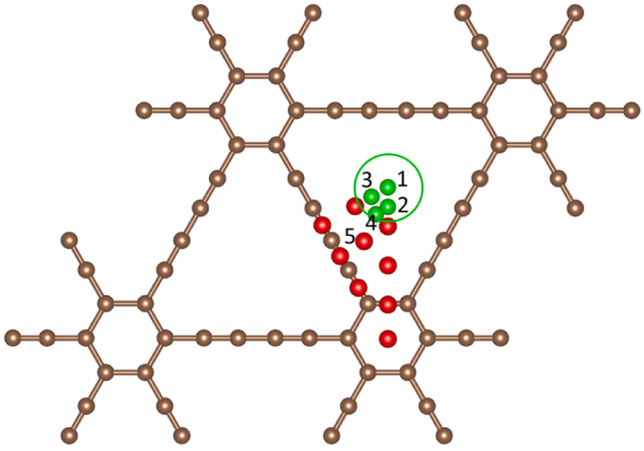

Fig. 1. Structure of GDY, with the brown spheres representing carbon atoms. The center of the pore is at ($x = 0$, $y = 0$, $z = 0$), and red and green dots represent the projections of the positions of the center of mass of the CO_2 molecule onto the GDY layer plane at the beginning of the MD simulations. The initial orientation of the axis of the molecule is perpendicular to the layer plane. Red and green colors indicate that the molecule bounces back or crosses to the other side of the layer, respectively. The green circle enclosing the green dots gives an estimation of the catching area.

velocities of the atoms of the layer at the end of the thermalization process at $T = 300$ K are used as the initial condition for the constant energy simulations of the filtering process.

Most simulations are run for a time of about 500 fs, with a time step of 1.935 fs. The total simulation time, under the conditions of the present simulations, is sufficiently long for the molecule to cross the membrane, or alternatively to reach the layer and bounce back. In a few cases, longer simulation times have been employed to secure a clear conclusion in favor of crossing or non-crossing through the pore.

3. CO_2 through GDY

With the GDY layer in its lowest energy configuration at $T = 0$ K, the constant-energy MD simulations begin by placing the center of mass of the CO_2 molecule at different positions (x, y, $z = 4$) above the GDY layer. The projections of those initial positions onto the layer plane, that is, their (x, y) coordinates, have been plotted in Fig. 1 as green and red dots. The sampling of initial (x,y) positions has been selected to cover the whole area of the pore, more precisely to cover the triangular region of the pore irreducible by rotational or reflection symmetry. The ($x = 0, y = 0$, $z = 0$) point is identified with the center of the pore. The initial orientation of the molecular axis is perpendicular to the GDY plane, but the orientation can change during the simulation. The starting velocity of the molecules has the vertical direction towards the layer, and a value $v = 0.0219$ Å/fs, which corresponds to a kinetic energy $E_k = 1.09$ eV. The zero-point vibrational energy of the molecule (0.311 eV) is taken into account by preparing the initial state of the molecule as a superposition of maximum elongations along the directions of all vibrational modes (both stretching and bending). The maximum elongations correspond to the zero-point energy of each mode. Of course, the molecules are able to execute all types of vibrational moles (stretching and bending) as the simulation proceeds. In specific cases, to be discussed below, the molecules started from a greater height z.

The simulations can be separated in two groups. In a first group, the molecules collide with the layer and bounce back, because in their approach to the layer the molecules reach distances from the carbon chains small enough to feel the repulsive part of the interaction potential. These molecules have initial positions whose projections on the GDY plane correspond to the red dots in Fig. 1. In contrast, the second group is formed by molecules that cross through the pore and pass to the other side. Their initial positions have (x, y) projections indicated by the dots in green color (dots labelled 1 to 4), and it can be noticed that those projections are sufficiently far from the carbon chains outlining the borders of the pore. Although DFT calculations predict that in this case there is a small activation energy barrier to cross to the other side of the layer [25], the kinetic energy of the molecules is high enough to overcome the barrier. In their fly to cross through the pore, the molecules of cases 2, 3, and 4 deviate a bit from the original vertical path and move towards the center of the pore. The orientation of the molecular axis changes during the fly, but the axis is perpendicular to the GDY layer at the time of crossing. The atomic structure of the GDY layer is deformed a little (or nothing) when these molecules cross through the pore, and fully recovers afterwards. Fig. 2 shows several snapshots along the crossing trajectory for the case labelled 3 in Fig. 1.

The evolution of the total potential energy of the system, E_p, with time is shown in Fig. 3 for the case in which the CO_2 molecule is initially placed above the center of the pore ($x = 0$, $y = 0$) at a sufficiently large distance from the GDY layer ($z = 7$ Å) so that the interaction between molecule and membrane is negligible [25]. This figure serves to clarify the evolution of the system in the initial stages of the simulations until the molecule crosses the membrane. At the beginning of the simulation the GDY layer is in its ground state configuration at temperature $T = 0$ K, and the CO_2 molecule has the zero-point energy, ZPE = 0.311 eV. For convenience, the reference of zero potential energy is set to the sum of the ground state energies (not including ZPE's) of isolated CO_2 and GDY (a similar definition is used for other systems). Therefore, the potential

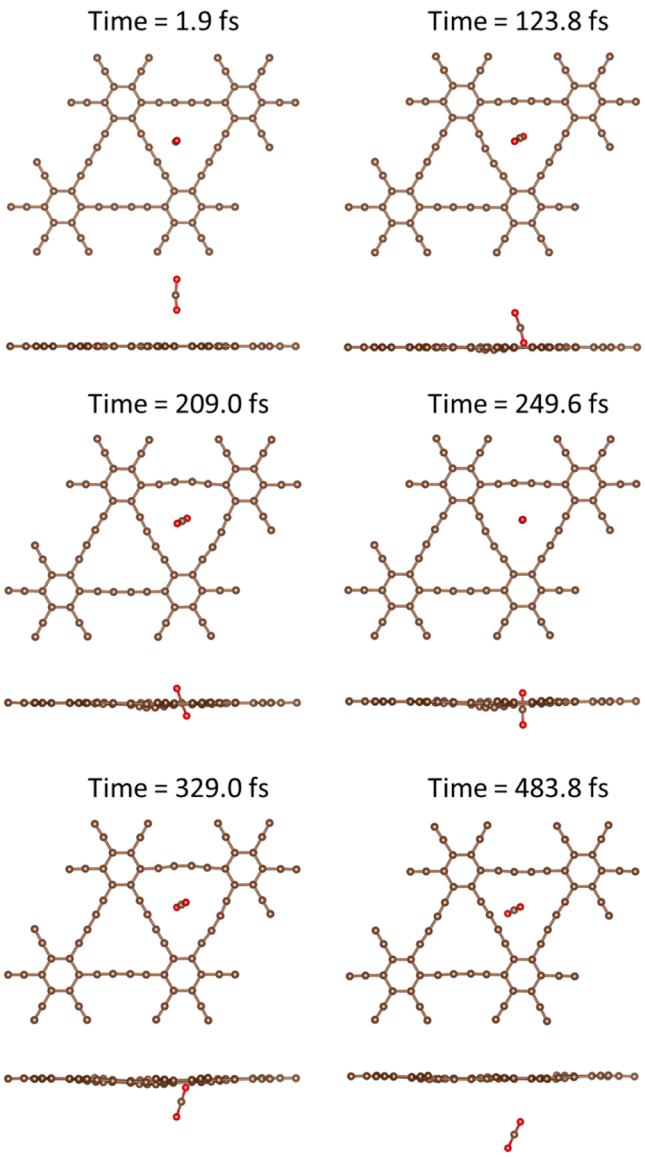

Fig. 2. Top and side views of several snapshots for increasing time, taken from a simulation corresponding to case labelled 3 in Fig. 1. The molecule approaches the pore and crosses to the other side.

energy at $t = 0$ in Fig. 3 is non zero, but equal to the ZPE of CO_2. The high-frequency oscillations of the potential energy observed in the Figure are essentially due to the vibrational motion of CO_2. By looking at the global behavior of the potential energy, there is an initial lowering of E_p, corresponding to the molecule approaching to the distance $z = 2.3$ Å from the layer, at which the interaction potential between CO_2 and GDY versus z has a minimum [25]. E_p then increases, indicating that the molecule is climbing the activation barrier to cross to the other side of the layer. The height of this dynamical activation barrier, about 0.26 eV, is in good agreement with the value obtained in the static DFT calculations for CO_2 molecules crossing close to the pore center [25]. After crossing the barrier, E_p decreases, revealing that the molecule goes through the minimum of the interaction potential on the other side of the layer. Finally, E_p rises again as the molecule escapes from that energy minimum.

The escape from that minimum is better seen in Fig. 4, which also serves to compare three simulations, corresponding to the cases labelled 1, 2, and 3 in Fig. 1. These simulations start with the molecule at $z = 4$ Å. The behavior of E_p in simulations 2 and 3 is rather similar to that in simulation 1, but a small time delay in crossing the membrane is

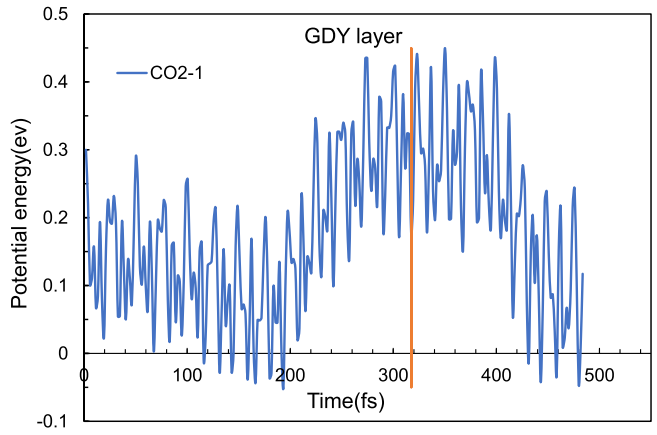

Fig. 3. Potential energy of the system as a function of time for a simulation (case 1 in Fig. 1) in which the CO_2 molecule crosses to the other side of the layer. The initial orientation of the molecular axis is perpendicular to the GDY plane, and the molecule starts at height $z = 7$ Å above the layer. The temperature of the GDY layer at the beginning of the simulation is $T = 0$ K. The vertical bar marks the time when the molecule crosses the pore, as visually observed in movies prepared from the data collected in the dynamical simulation.

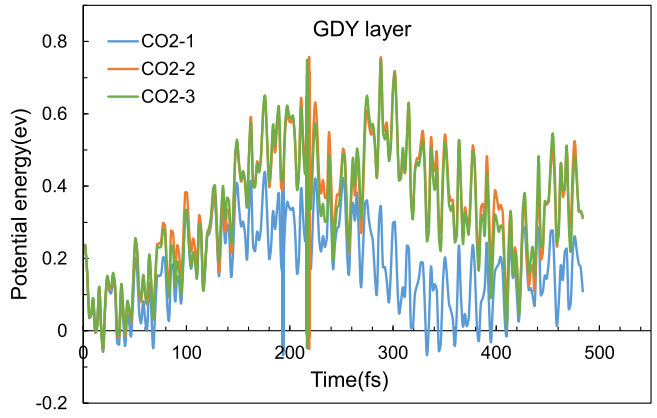

Fig. 4. Potential energy of the system as a function of time for three simulations (cases labelled 1, 2, 3 in Fig. 1) in which the CO_2 molecules cross to the other side of the layer. The initial orientation of the molecular axis is perpendicular to the GDY plane, and the molecules start at $z = 4$ Å. The temperature of the GDY layer at the beginning of the simulations is $T = 0$ K. The vertical bars mark the time when the molecules cross the pore.

observed. Since the CO_2 molecules are initially slightly off-center in simulations 2 and 3, their interaction with the borders of the pore is more intense, some energy is transferred to the GDY layer and this leads to a small distortion of those borders. In order to facilitate the crossing to the other side, the molecule deviates from its original vertical path and moves a bit towards the optimal path through the center of the pore. This results in the small time delay in crossing to the other side (the crossing times, obtained from movies prepared from the dynamical simulations, are indicated by the vertical bars), and in higher dynamical crossing barriers. These arguments are supported by the results obtained by Rafiei et al. on the interaction of small molecules (O_2, N_2) with GDY [24]. These authors have shown that the form of the interaction potential in the layer plane, namely as a function of x (or y) and constant $z = 0$, is approximately parabolic. The interaction becomes highly repulsive as x or y deviates from the pore center; that is, as the molecules approach the carbon chains in the borders of the pore. Consequently, the height of the activation barrier to cross to the other side of the layer is larger when the initial path of the molecule deviates from an ideal path through the center of the pore, and this motivates the molecules to deviate towards a path closer to the center of the pore. The higher potential energies after 150 fs observed in Fig. 4 for these two simulations are due to the energy absorbed by the GDY layer, which results in a small layer deformation. This deformation produces an additional feature: a low-frequency oscillation of the potential energy (well distinguished from the high-frequency oscillations associated with CO_2 vibrations), which reveals the return of the deformed GDY layer to its original structure.

In the simulations associated with the red dots in Fig. 1, the incoming molecules rebound because in their flight those molecules sample the hardest repulsive part of the interaction potential with the pore borders. The collision induces bending of the carbon chains, which later on recover. The potential energy of the system is plotted in Fig. 5 for one of the simulations in which the molecule bounces back (simulation 5 in Fig. 1), and the differences with respect to Fig. 4 are evident. The oscillations of the GDY layer in response to the collision are revealed by the low frequency oscillations of the potential energy in Fig. 5. Some snapshots of the structure of the system along the simulation are shown in Fig. 6.

In summary, the crossing of molecules through the pore follows a funnel mechanism. There is a catchment area (the wide part of the funnel), such that incoming molecules falling into the catchment area move towards the narrow part at the bottom of the funnel and cross the pore. The green circle drawn in Fig. 1 gives an estimation of the catchment area, which in the case of GDY is small because the effective size of the pore is small. The catchment area has been estimated by the analysis of simulations which start with the CO_2 molecule at a height $z =$ 4 Å. This estimation is reasonable, because simulations starting at higher height z lead to the same catchment area.

Simulations were also run with the axis of the molecule parallel to the GDY plane. All those molecules bounced back after colliding with the layer, even in the case when the projection of the center of mass of the molecule coincides with the center of the pore ($x = 0, y = 0$). This is due to the relative sizes of the molecule and pore. The shape of the linear CO_2 molecule, accounting for the electronic cloud, is elongated (approximately cylindrical) [42], and when CO_2 arrives at the pore with its axis parallel to the layer plane, the size of the molecule is too large to fit into the pore area and pass to the other side; one has to notice that the effective empty area of the pore is smaller than the geometrical area, because of the extension of the electronic cloud of the carbon chains. This is appreciated in Fig. 7, where the electron density of the system when the center of mass of the CO_2 molecule is at ($x = 0, y = 0, z = 0$), that is, at the center of the pore in the layer plane, has been plotted for two orientations of the molecular axis, perpendicular and parallel to the layer. The overlap of the electron densities is quite substantial for the

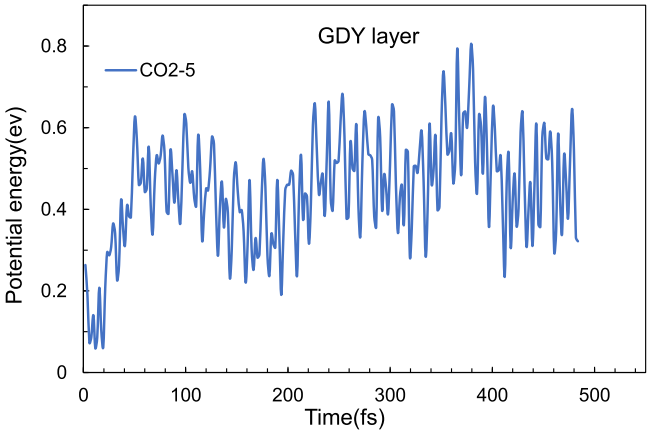

Fig. 5. Potential energy as a function of time for a simulation (case 5 in Fig. 1) in which CO_2 collides with GDY and bounces back. The molecule starts at $z = 4$ Å, and the initial orientation of its axis is perpendicular to the GDY plane. The temperature of GDY at the beginning of the simulations is $T = 0$ K.

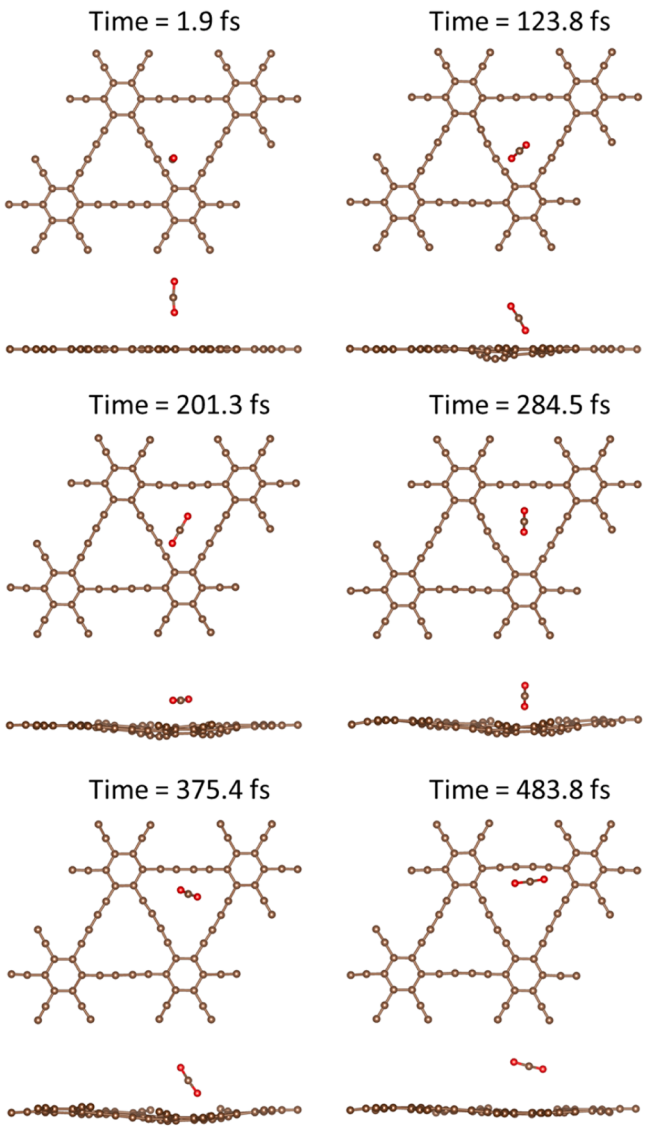

Fig. 6. Top and side views of several snapshots for increasing time, taken from the simulation corresponding to case labelled 5 in Fig. 1. The molecule collides with the layer, and bounces back.

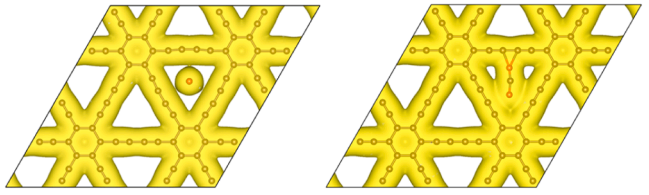

Fig. 7. Top view of the electron density when the CO_2 molecule is on the layer plane of GDY. The molecule is placed at the center of the pore, with the axis perpendicular (left panel) and parallel (right panel) to the layer plane. The yellow regions correspond to surfaces of constant electron density with the value 0.01 *e*/a.u.^{3}.

parallel orientation, and since the value of the contour plotted, 0.01 *e*/a.u.^{3}, is not small, this reveals that the molecule is sampling the repulsive part of the interaction potential with the carbon chains. In contrast, the plot for the perpendicular orientation shows that the CO_2 molecule just fits into the pore. This highlights the critical importance of the orientation of the molecular axis to allow for crossing.

Simulations with the GDY layer initially equilibrated at $T = 300$ K deliver results quite similar to those obtained with the layer at $T = 0$ K, because the pore size practically does not change. All the simulations starting with the molecular axis parallel to the GDY layer led to the bouncing back of the molecules. In contrast, the molecule crossed to the other side in some simulations with the axis perpendicular to the layer. The catchment area is practically the same as that for initial $T = 0$ K. The small differences between the simulations at the two temperatures are illustrated in Fig. 8 for the case when the molecule is initially above the center of the pore (corresponding to dot 1 in Fig. 1). The crossing of the layer, observed in the movies prepared from the simulations, and marked by the vertical bars in Fig. 8, occurs at the same time in the two cases (initial $T = 0$ K, and $T = 300$ K). The shapes of the potential energy curves reveal that the GDY layer is not perturbed during the crossing of the molecule at $T = 0$ K. The potential energy curve when the GDY layer is initially at $T = 300$ K is similar, showing well the maximum associated to the barrier crossing, and the two minima associated to the minima of the interaction potential on the two sides of the barrier. However, weak irregularities can be observed in the potential energy curve, revealing the thermal motion of the atoms of the GDY layer. This thermal motion is responsible for the larger potential energies in the simulation at initial $T = 300$ K.

The information contained in the plots of the potential energy throughout the MD simulations can be presented in an alternative way: plotting the potential energy as a function of the vertical distance z between the molecule and the membrane layer. This is done in Fig. S1 for a simulation corresponding to case 4 in Fig. 1, with the initial orientation of the axis of the CO_2 molecule perpendicular to the GDY plane. Figure S1 shows that the plots of potential energy versus t or

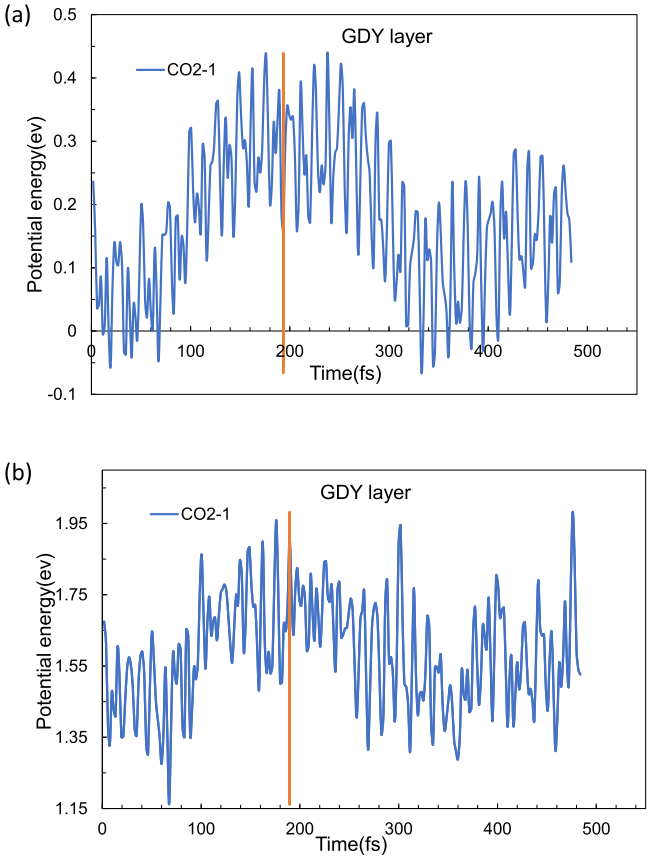

Fig. 8. Potential energy of the system as a function of time for simulations in which the CO_2 molecule is initially above the center of the pore, with the molecular axis perpendicular to the layer plane. The GDY layer is initially at $T = 0$ K in panel (a), and at $T = 300$ K in panel (b). The vertical red lines mark the time of barrier crossing.

versus z, both provide a clear interpretation of the permeation process.

4. CH_4 through GDY

CH_4 is a molecule with the H atoms in tetrahedral configuration around the central C atom. The distribution of its electron density in space is close to spherically symmetric [42], and then the orientation of the molecule in the simulations is irrelevant. With the GDY layer initially a $T = 0$ K, simulations started with the center of mass of the molecule positioned 4 Å above the geometric center of the pore ($x = 0, y = 0$). A first simulation was run with initial velocity $v = 0.0219$ Å/fs in the vertical direction towards the layer. This is the same velocity employed for CO_2. The corresponding translational kinetic energy of CH_4 is $E_k = 0.396$ eV. The molecule collided with the GDY layer and bounced back. One can notice that the kinetic energy of the molecule is lower than the static crossing barrier of 0.52 eV, calculated by Mahnaee et al. [25].

A higher kinetic energy of 1.09 eV was then used, which is the kinetic energy in the simulations for CO_2. The corresponding initial velocity of the molecule is $v = 0.0363$ Å/fs. Interestingly, the CH_4 molecule also bounced back. The explanation is that the dynamical barrier to cross to the other side is larger than the static barrier obtained from DFT calculations [25], and the larger barrier prevents the crossing. The kinetic energy was further increased to $E_k = 1.50$ eV ($v = 0.0426$ Å/fs), and in that case the molecule crossed to the other side of the GDY layer. This kinetic energy is substantially higher than the kinetic energy in the simulations for CO_2, and this reveals that the crossing of CO_2 through the pores of GDY is easier than the crossing of CH_4, and that GDY pores discriminate well between the two molecules.

The size of the CH_4 molecule makes its passing through the triangular pores of GDY already difficult, as shown in Fig. 9. In addition, the vibrational motion of the molecule and of the atoms of the carbon chains enhances the overlap between the high electron density regions of the electron clouds of CH_4 and GDY, which are responsible of the repulsive part of the interaction potential. Since starting positions ($x = 0, y = 0$, z) are the most favorable ones concerning the possibility of crossing the pore, and even in this case the CH_4 molecule bounces back, other starting positions with (x, y) projections off the geometrical center of the pore are even more unfavorable, and the molecules also bounce back.

5. CO_2 through BGDY

The area of the hexagonal pores in BGDY is much larger than the area of the triangular pores in GDY. For this reason, the crossing of small molecules through the layer is expected to be easier [25]. Constant energy simulations were performed with the molecule initially 4 Å above the layer, and having (x, y) coordinates such that their projections on the layer plane correspond to the dots inside the hexagon plotted in Fig. 10. Simulations were run with the molecular axis perpendicular and parallel to the BGDY plane. The initial structure of the membrane corresponds to its ground state configuration at $T = 0$ K and $T = 300$ K. The initial

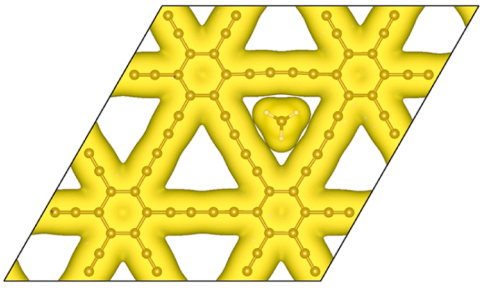

Fig. 9. Top view of the electronic density when the CH_4 molecule is on the layer plane of GDY. The molecule is placed at the center of the triangular pore. The yellow regions correspond to a surface of constant electron density with the value 0.01 e/a.u.^{3}.

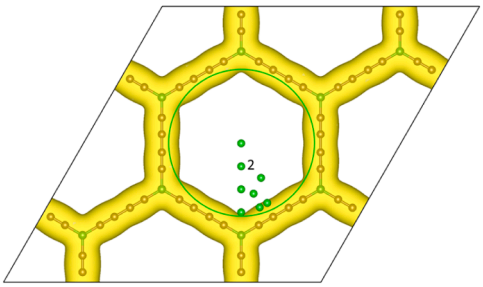

Fig. 10. Structure of BGDY, with the green and brown spheres in the chains representing B and C atoms, respectively. Yellow regions represent surfaces of constant electron density with the value 0.01 e/a.u.^{3}. The center of the pore is at ($x = 0, y = 0, z = 0$). The green dots inside the hexagonal pore mark the projections of the center of mass of the CO_2 molecules onto the BGDY plane at the beginning of the MD simulations. The green color of the dots indicates that the molecules cross to the other side in all the simulations, independently of the orientation of the molecular axis. The area inside the green circle represents the catching area of the pore.

velocity was $v = 0.0219$ Å /fs. In all cases the molecule crossed to the other side of the layer.

In most simulations the CO_2 molecules change their flying path and move towards the pore center as a way to avoid the repulsive interaction with the carbon chains. However, the BGDY structure deforms a bit and suffers local bending when the projections of the initial positions of the molecules are not near ($x = 0, y = 0$). In these cases, the orientation of the molecular axis changes during the fly, and the molecules may rotate. This is displayed in Fig. 11, which shows the behavior of the angle θ between the axis of the CO_2 molecule and the z axis for a simulation in which the CO_2 molecule starts near the border of the catchment area. The evolution of θ over time reveals a significant variation of the molecular orientation during the simulation. The permeation of pure gases through nanoporous graphene membranes, modeled as holes in graphene, has been investigated by Guo et al. [43] using MD based on empirical potentials, and the molecular reorientation was also noticed.

These results are consistent with our previous static DFT calculations, which predicted that there is no activation barrier for CO_2 crossing near the center of the pores in the BGDY layer [25]. Those DFT calculations also revealed that the potential energy as a function of z has a minimum of depth 0.12 eV in the region around $z = 0$. The lack of an activation barrier and the presence of the shallow energy minimum can be appreciated in the potential energy plotted in Fig. 12 for a MD simulation corresponding to case labelled 2 in Fig. 10, with the

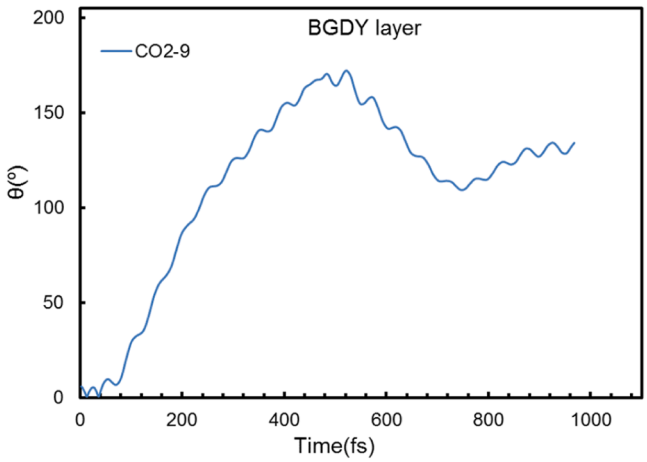

Fig. 11. Angle θ between the axis of the CO_2 molecule and the z axis as a function of simulation time, for a simulation in which the CO_2 molecule starts near the border of the catchment area of BGDY.

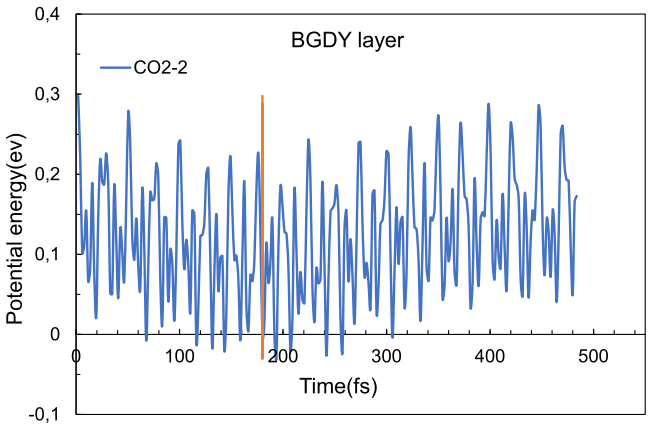

Fig. 12. Potential energy as a function of time for a simulation in which the initial orientation of the molecular axis of the CO_2 molecule is perpendicular to the BGDY plane. The BGDY layer is initially at $T = 0$ K. The simulation corresponds to case 2 in Fig. 10. The red vertical bar marks the time of crossing through the layer.

molecular axis perpendicular to the membrane. In the simulations with the BGDY layer initially at $T = 300$ K, the results are similar to those at $T = 0$, and the only observable difference is the thermal motion of the membrane atoms.

A feature common to the two initial temperatures is that molecules with starting (x, y) coordinates not close to ($x = 0$, $y = 0$) show a time delay in crossing the layer in comparison to molecules with starting coordinates near ($x = 0$, $y = 0$). The time delay is larger the more the initial (x, y) coordinates deviate from (0, 0). This again gives evidence of the funnel mechanism, even more distinctly than for GDY, because the catching area, which is estimated as the area inside the green circle in Fig. 10, is much larger. The CO_2 molecules are collected in the catching area, but cross through the membrane near the center of the pore.

6. CH_4 through BGDY

Simulations started with the CH_4 molecule situated 4 Å above the layer, and having (x, y) coordinates with projections on the layer plane represented by the dots in Fig. 13. The initial velocity was $v = 0.0219$ Å /fs. The red and green dots correspond to simulations in which the molecules bounce back or pass to the other side, respectively. In the simulations labelled 3, 4, and 5, the molecules deviate from their original vertical path and move towards the center, which leads to a time delay in crossing to the other side compared to simulations 1 and 2. That is, the permeation of the molecules through the pore follows the funnel mechanism. This occurs independently of the initial temperature of the

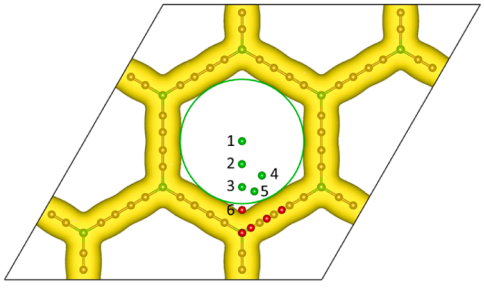

Fig. 13. Projection of the initial positions of the center of mass of the CH_4 molecule onto the layer plane of BGDY. The yellow regions correspond to a surface of constant electron density with the value 0.01 e/a.u.^{3}. Red and green dots indicate that molecules bounce back or cross to the other side of the BGDY layer, respectively. The green circle enclosing the green dots gives an estimation of the catching area of the funnel.

BGDY layer, $T = 0$ K, or $T = 300$ K. In the simulation labelled 6, the CH_4 molecule bounces back. To investigate case 6 in more detail, simulations with higher velocities, $v = 0.0363$ Å /fs and $v = 0.0426$ Å /fs, corresponding to kinetic energies $E_k = 1.09$ eV and $E_k = 1.50$ eV, respectively, were run, and the result is that the molecule also bounces back at those higher kinetic energies. In summary, both CO_2 and CH_4 manage to cross the pores of the BGDY layer. But, the comparison of Figs. 10 and 13 reveals that the catchment area is larger for CO_2, a feature consistent the results obtained for GDY.

7. Discussion

Although static DFT calculations provide interesting information on the filtering of gases through GDY and BGDY monolayer membranes [25], MD-DFT simulations offer a faithful picture of the on-the-fly interaction between molecules and membranes, and describe in detail the dynamical processes of crossing through the pore or turning back. A significant, relatively large number of simulations have been performed considering that the DFT-MD simulations are computationally very demanding and, therefore, the number of calculated trajectories is necessarily limited. However, a careful selection of initial conditions for the molecules and membranes allowed us to unravel the permeation mechanism of CO_2 and CH_4 molecules through GDY and BGDY layers. To make the atomistic simulations more realistic, we have taken into account the flexibility of the nanoporous membranes; that is, the fact that the membrane may deform as a result of the impact of the incoming molecules. The importance of considering membrane flexibility was confirmed by Guo et al. [44] for the case of the permeation of pure gases (H_2, O_2, N_2, CO_2, CH_4) through single-layer porous graphene.

The main factor controlling the crossing of CO_2 and CH_4 molecules through porous GDY and BGDY is the relative size of molecule and pore. The effective size of the pore is smaller than the geometrical size, because the carbon chains bounding the pore have a thickness, originating from the extension of the electron density cloud, which decays exponentially in the outer part of atoms or molecules [45,46]. The incoming molecules cannot go through regions of the membrane where the electron density is high; that is, close to the carbon chains. This is because the overlap between the high density parts of the electronic clouds of molecule and membrane samples the repulsive part of the interaction potential. We have found reasonable to characterize the thickness of the carbon chains as the region bounded by density contours with a value of 0.01 e/a.u.^{3}. This value has been selected by comparing several pictures, similar to Figs. 7 and 9, for electron density contours 0.01, 0.007, and 0.005 e/a.u.^{3} (see Fig. S2 in the Supplementary Information). The results are not too different, and a density cutoff of 0.01 e/a.u.^{3}, which leads to an effective triangular pore of length size equal to 5.31 Å, appears to reflect better the effective size of the pore. A different measure of the effective size of GDY pores was used by Jiao et al. [19] and Cranford and Buehler [17] in a computational study of the purification of H_2 in mixtures of H_2, CO and CH_4. In those works, the pore was defined as the region beyond the van der Waals radius of the carbon atoms in the diacetylenic chains. This leads to triangular pores with side-length 3.8 Å. In a simulation of hydrogen purification through a porous C_2N membrane, Xu et al. [47] defined the effective pore size using electron density contours of 0.007 e/a.u.^{3}.

The MD simulations reveal that the molecules follow an interesting process to permeate through the pores. This is a *funnel* mechanism. The pore is characterized by a catchment area (the wide area region at the top of the funnel), which is roughly mimicked by the circles drawn in Figs. 1, 10 and 13. Molecules which in their motion towards the membrane fall inside that catchment area will cross the pore. However, in their approach to the membrane the molecules deviate from their original flying path and move towards the central region of the pore (the narrow part at the bottom of the funnel). Fig. 14 illustrates the funnel mechanism for a simulation in which a CO_2 molecule starts at a position near the border of the catchment area (see Fig. 10); that is, with (x, y)

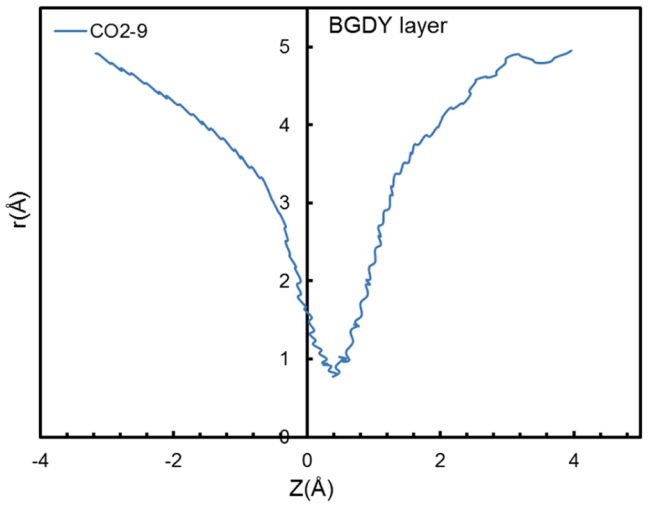

Fig. 14. Radial coordinate r of the center of mass of the CO_2 molecule, defined as $r = (x^2 + y^2)^{1/2}$, versus the vertical distance z to the BGDY layer plane, for a simulation in which the molecule starts near the border of the catchment area; that is, far from ($x = 0$, $y = 0$). As z decreases, the value of r decreases, displaying the funnel mechanism. Positive and negative values of z, represent distances to the GDY layer before and after the molecule crosses through the membrane pore, respectively.

coordinates far from (0, 0). Fig. 14 shows the radial coordinate r of the center on mass of the molecule, defined as $r = (x^2 + y^2)^{1/2}$, versus the vertical distance z to the BGDY layer plane. At each specific time during the simulation, r represents the distance between the molecule and a vertical line passing through the pore center (0,0). Then, the decreasing behavior of r displayed in Fig. 14 means that, in its motion, the molecule is approaching the pore center (although the pore is not crossed at ($x = 0$, $y = 0$)). After crossing the pore, the molecule scatters with increasing r. Fig. S3 shows the funnel effect in a complementary plot of r versus time. In addition, Fig. S4 displays the funnel effect for the passing of CO_2 through GDY.

When the nanopore area is large, like in BGDY, the catchment area is also large and the permeation behavior of CO_2 and CH_4 is not too different. But when the membrane is formed by narrow nanopores, as in the case of GDY, the CO_2 molecules have a crucial advantage arising from the anisotropic shape of the molecule. The linear CO_2 molecule can orient its axis perpendicular to the plane of the GDY layer, and in this way its effective size decreases and the molecule can cross through narrow pores. Instead, the size of the quasi-spherical CH_4 molecules is the same, independent of the orientation.

The analysis of the potential energy of the system along the simulation runs gives detailed insight into the processes of pore crossing or bouncing back of the molecules. It reveals that, as a result of the interaction between molecule and membrane, the structure of the monolayer membrane deforms a bit in most cases, and later on returns to its original form. Another feature uncovered by the dynamical simulations is the importance of the vibrational motion of the gas molecules on the permeation process. When the size of the molecule is close to the effective size on the pore, as occurs for CH_4 colliding with GDY, the periodic enhancement of the C—H bond lengths, arising from the vibrational motion of the molecule, increases its effective dynamical size, and the permeation through the pores becomes reduced.

The results obtained are based on molecular dynamics simulations in which the molecules start at a height of 4 Å above the membrane layer, except for some test cases starting at $z = 7$ Å. For separations beyond 4 Å, the only interaction between the molecules and the layer is the weak van der Waals tail [25]. This means that beyond 4–5 Å the incoming molecules are practically free, and simulations starting at those distances or larger will lead to essentially the same results. This can be seen in Fig. S5, which shows the potential energies for two simulations of the permeance of a CO_2 molecule with initial ($x = 0$, $y = 0$) and axis orientation perpendicular to the GDY layer. The molecules start at $z = 7$ Å, and $z = 4$ Å, respectively, and the Figure reveals that the behavior of the potential energy in the two curves is the same, except, obviously, between $z = 7$ Å and $z = 4$ Å. This confirms the free flight of the molecule between $z = 7$ Å and $z = 4$ Å, and guaranties that the results for the crossing and rebounding of the molecules, and for the catching area, obtained when the molecules start at $z = 4$ Å are trustable. Since DFT MD simulations have a high computational cost, restricting to starting heights $z = 4$ Å is then convenient.

A thermodynamic study of the permeances of CO_2 and CH_4 through a GDY membrane was performed in our previous work [25]. The permeances of these two molecules at room temperature (for an incoming pressure $p = 3 \times 10^5$ Pa, and a pressure difference between the two sides of the membrane $\Delta p = 105$ Pa) are a little above and a little below the industrial permeance limit of 6.7×10^{-9} mol m^{-2} s^{-1} Pa^{-1}, respectively. Attempting to simulate these conditions with ab initio MD is not realistic, because for the small kinetic energies associated to realistic industrial temperatures, the simulation times should be orders of magnitude larger. Well aware of these difficulties, our purpose in the present work has been to perform model MD simulations to focus on the elucidation of the physical mechanisms of the permeation process. The kinetic energies (or the velocities) in the model MD simulations have been chosen high enough to allow the full process of pore crossing (or rebounding) to occur in the course of the simulation runs. For this, evidently, the kinetic energies have to be larger than the activation barriers to cross through the pores.

The efficiency of a porous membrane to separate CO_2 and CH_4 (or other gas mixtures) depends on two main ingredients: selectivity and permeability. The selectivity

$$S(CO_2 / CH_4) = e^{-(E_b(CO_2) - E_b(CH_4))/k_B T} \quad (1)$$

depends exponentially on the difference between the two activation barriers for crossing the pore. In GDY, the crossing barriers are E_b (CO_2) = 0.26 eV (see also Fig. 3), and E_b (CH_4) = 0.52 eV [25]. That is, the barriers differ by a factor of 2, and consequently the selectivity is good. On the other hand, the selectivity of BGDY is unsatisfactory because the two barriers are essentially zero. The permeance of each type of molecule depends on the crossing barrier, but also on the size (or the catching area) of the pores, relatively small in GDY and large in BGDY. The catching area for CO_2 molecules in BGDY is larger than for CH_4, and the permeance of CO_2 will be higher. In summary, the balance between permeance and selectivity is quite delicate, but one can notice that in both GDY and BGDY the crossing of CO_2 through the pores will be easier.

Due to computational limitations associated to ab initio MD, the molecular trajectories have been restricted in such a way that the initial velocities have directions perpendicular to the layer membrane. The funnel mechanism suggests that a substantial part of the molecules arriving with non-perpendicular trajectories will also be collected and channeled through the funnels. In a theoretical investigation, Yuan and coworkers [48,49] have discussed the mechanisms of gas permeation through graphene nanopores. In addition to the direct-impingement pathway, they discuss the surface diffusion pathway, in which adsorbed molecules diffuse until reaching the pores. This interesting diffusion mechanism is natural in porous graphene, where there are sizable regions of unaltered (pristine) graphene between neighbor pores. But we expect the mechanism to be less important in GDY and BGDY, because the pores are so close to each other that the molecules always arrive at the membrane very near a pore, at least.

8. Summary and conclusions

Ab initio molecular dynamics simulations reveal the mechanisms of permeation of gas molecules (here CO_2 and CH_4) through the nanopores

of monolayer GDY and BGDY. The relative size of molecule and pore is the deciding factor for a successful permeation. The relevant size of the pore is not its geometric size, but a smaller effective size that accounts for the extent of the electronic cloud of the carbon chains forming the borders of the pore. Also crucial is the fact that the linear CO_2 molecule can advantageously orient its axis to facilitate pore crossing. The permeation through the nanopores of these layered materials follows a funnel mechanism, in which molecules collected in the catchment area of the pore (the wide region at the top of the funnel) deviate from their original path and cross the pore through a smaller region around the center of the pore, the narrow tube at the bottom of the funnel.

CRediT authorship contribution statement

Sahar Mahnaee: Writing – original draft, Visualization, Methodology, Investigation, Formal analysis. **María J. López:** Writing – review & editing, Visualization, Supervision, Project administration, Methodology, Investigation, Funding acquisition, Formal analysis, Conceptualization. **Julio A. Alonso:** Writing – review & editing, Writing – original draft, Supervision, Methodology, Investigation, Formal analysis, Conceptualization.

Declaration of competing interest

The authors declare that they have no known competing financial interests or personal relationships that could have appeared to influence the work reported in this paper.

Acknowledgements

Work supported by Ministerio de Ciencia e Innovación of Spain (grant PID2022-138340OB-I00 funded by MCIN/AEI/ 10.13039/501100011033 and FSE+), Junta de Castilla y León (Apoyo a GIR, Project VA029G24), and University of Valladolid (GIR Nanostructures Physics Group). S. M. acknowledges a predoctoral grant with the University of Valladolid, and J. A. A. acknowledges the hospitality of DIPC.

Supplementary materials

Supplementary material associated with this article can be found, in the online version, at doi:10.1016/j.surfin.2025.107127.

Data availability

Data will be made available on request.

References

[1] C. Song, Global challenges and strategies for control, conversion and utilization of CO_2 for sustainable development involving energy, catalysis, adsorption and chemical processing, Catal. Today 115 (2006) 2–32, https://doi.org/10.1016/j.cattod.2006.02.029.

[2] S. Choi, J.H. Drese, C.W. Jones, Adsorbent materials for carbon dioxide capture from large anthropogenic point sources, ChemSusChem 2 (2009) 796–854, https://doi.org/10.1002/cssc.200900036.

[3] J. Saavedra, L. Merino, V. Kafarov, Determination of the gas composition effect in carbon dioxide emission at refinery furnaces, Chem. Eng. Transact. 35 (2013) 1357–1362, https://doi.org/10.3303/CET1335226.

[4] S. Wang, Z. Cao, L. Li, N. Wu, L. Huang, S. Zuo, X. Lu, CO_2/CH_4 separation via carbon-based membrane: the dynamic role of gas-membrane interface, Langmuir 38 (2022) 11274–11283, https://doi.org/10.1021/acs.langmuir.2c01333.

[5] A. Ali, M. Aamir, K.H. Thebo, J. Akhtar, Laminar graphene oxide membranes towards selective ionic and molecular separations: challenges and progress, Chem. Record 19 (2019) 1–12, https://doi.org/10.1002/tcr.201900024.

[6] P. Bernardo, E. Drioli, G. Golemme, Membrane gas separation: a review/state of the art, Ind. Eng. Chem. Res. 48 (2009) 4638–4663, https://doi.org/10.1021/ie8019032.

[7] S. Blankenburg, M. Bieri, R. Fasel, K. Müllen, C.A. Pignedoli, D. Passerone, Porous graphene as an atmospheric nanofilter, Small 6 (2010) 2266–2271, https://doi.org/10.1002/smll.201001126.

[8] H.W. Kim, H.W. Yoon, S.M. Yoon, B.M. Yoo, B.K. Ahn, Y.H. Cho, H.J. Shin, H. Yang, U. Paik, S. Kwon, J.Y. Choi, H.B. Park, Selective gas transport through few-layered graphene and graphene oxide membranes, Science 342 (6154) (2013) 91–95, https://doi.org/10.1126/science.1236098.

[9] N. Razmara, A. Kirch, J. Romano Meneghini, C. Rodrigues Miranda, Efficient CH_4/CO_2 gas mixture separation through nanoporous graphene membrane designs, Energies 14 (2021) 2488, https://doi.org/10.3390/en14092488.

[10] X. Gao, H. Liu, D. Wang, J. Zhang, Graphdiyne: synthesis, properties, and applications, Chem. Soc. Rev. 48 (2019) 908–936, https://doi.org/10.1039/C8CS00773J.

[11] Y. Du, W. Zhou, J. Gao, X. Pan, Y. Li, Fundament and application of graphdiyne in electrochemical energy, Acc. Chem. Res. 53 (2010) 459–469, https://doi.org/10.1021/acs.accounts.9b00558.

[12] N. Wang, X. Li, Z. Tu, F. Zhao, J. He, Z. Guan, C. Huang, Y. Yi, Y. Li, Synthesis and electronic structure of borongraphdiyne with *An sp*-hybridized carbon skeleton and its application in sodium storage, Angewand. Chem. Int. Edit. 57 (2018) 3968–3973, https://doi.org/10.1002/anie.201800453.

[13] A. Ali, R. Pothu, S. Siyal, S. Phulpoto, M. Sajjad, K. Thebo, Graphene-based membranes for CO_2 separation, Mater. Sci. Energy Technolog. 3 (2019) 83–88, https://doi.org/10.1016/J.MSET.2018.11.002.

[14] C. Sun, B. Wen, B. Bai, Application of nanoporous graphene membranes in natural gas processing: molecular simulations of CH_4/CO_2, CH_4/H_2S and CH_4/N_2 separation, Chem. Eng. Sci. 138 (2015) 616–621, https://doi.org/10.1016/J.CES.2015.08.049.

[15] M. Bartolomei, E. Carmona-Novillo, M.I. Hernández, J. Campos-Martínez, F. Pirani, G. Giorgi, Graphdiyne pores: ‘‘ad hoc’’ openings for helium separation applications, J. Phys. Chem. C 118 (2014) 29966–29972, https://doi.org/10.1021/jp510124e.

[16] E. García-Arroyo, M. Campos-Martínez, M. Bartolomei, F. Pirani, M.I. Hernández, Molecular hydrogen isotope separation by a graphdiyne membrane: a quantum mechanical study, Phys. Chem. Chem. Phys. 24 (2022) 15840–15850, https://doi.org/10.1039/D2CP01044E.

[17] S.W. Cranford, M.J. Buehler, Selective hydrogen purification through graphdiyne under ambient temperature and pressure, Nanoscale 4 (2012) 4587–4593, https://doi.org/10.1039/C2NR30921A.

[18] K. Xu, N. Liao, M. Zhang, W. Xue, Atomic-scale investigations of enhanced hydrogen separation performance from doping boron and nitrogen in graphdiyne membrane, Int. J. Hydrog. Energy 45 (2020) 28893–28902, https://doi.org/10.1016/j.ijhydene.2020.07.174.

[19] Y. Jiao, A. Du, M. Hankel, Z. Zhu, V. Rudolph, S.C. Smith, Graphdiyne: a versatile nanomaterial for electronics and hydrogen purification, Chem. Commun. 47 (2011) 11843–11845, https://doi.org/10.1039/C1CC15129K.

[20] X. Zhang, R. Fang, D. Chen, G. Zhang, Using Pd-doped graphyne to detect dissolved gases in transformer oil: a density functional theory investigation, Nanomaterials 9 (2019) 1490, https://doi.org/10.3390/nano9101490.

[21] Z. Meng, X. Zhang, Y. Zhang, H. Gao, Y. Wang, Q. Shi, D. Rao, Y. Liu, K. Deng, R. Lu, Graphdiyne as a high efficiency membrane for separating oxygen from harmful gases: a first-principles study, ACS Appl. Mater. Interface. 8 (2016) 28166–28170, https://doi.org/10.1021/acsami.6b08662.

[22] P. Rezaee, H.R. Naeij, A new approach to separate hydrogen from carbon dioxide using graphdiyne-like membrane, Sci. Rep. 10 (2010) 13549, https://doi.org/10.1038/s41598-020-69933-9.

[23] Z. Zhou, Y. Tan, Q. Yang, A. Bera, Z. Xiong, M. Yagmurcukardes, M. Kim, et al., Gas permeation through graphdiyne-based nanoporous membranes, Nat. Commun. 13 (2022) 403, https://doi.org/10.1038/s41467-022-31779-2.

[24] M.A. Rafiei, J. Campos-Martínez, M. Bartolomei, F. Pirani, A. Maghari, M. I. Hernández, Separation of oxygen from nitrogen using a graphdiyne membrane: a quantum-mechanical study, Phys. Chem. Chem. Phys. 26 (2024) 24553–24563, https://doi.org/10.1039/d4cp02287d.

[25] S. Mahnaee, M.J. López, J.A. Alonso, Separation of CO_2/CH_4 gas mixtures using nanoporous graphdiyne and boron-graphdiyne membranes: influence of the pore size, Phys. Chem. Chem. Phys. 26 (2024) 15916–15926, https://doi.org/10.1039/d4cp00872c.

[26] S. Plimpton, Fast parallel algorithms for short-range molecular dynamics, J. Comput. Phys. 117 (1995) 1–19, https://doi.org/10.1006/jcph.1995.1039.

[27] J. Guo, G. Galliéro, R. Vermorel, Modeling gas permeation mechanisms through 2D membranes: comparison between a phenomenological model and extensive molecular simulations, J. Chem. Phys. 157 (2022) 224704, https://doi.org/10.1063/5.0128632.

[28] F. Cabrales-Navarro, J. Gomez-Ballesteros, P. Balbuena, Molecular dynamics simulations of metal-organic frameworks as membranes for gas mixtures separation, J. Memb. Sci. 428 (2013) 241–250, https://doi.org/10.1016/J.MEMSCI.2012.10.058.

[29] M. Heiranian, A.B. Farimani, N.R. Aluru, Water desalination with a single-layer MoS_2 nanopore, Nat. Commun. 6 (2015) 8616, https://doi.org/10.1038/ncomms9616.

[30] M. Ganji, R. Dodangeh, Hydrogen purification performance of a nanoporous hexagonal boron nitride membrane: molecular dynamics and first-principle simulations, Phys. Chem. Chem. Phys. 19 (2017) 12032–12044, https://doi.org/10.1039/c7cp01665d.

[31] L. He, Y. Pan, T. Wang, L. Yu, Molecular simulation and optimization on the microporous structure in carbon molecular sieve membrane for CO_2/CH_4 separation, Chem. Phys. Lett. 738 (2020) 136910, https://doi.org/10.1016/j.cplett.2019.136910.

[32] W. Kohn, L.J. Sham, Self-consistent equations including exchange and correlation effects, Phys. Rev. 140 (1965) A1133–A1138, https://doi.org/10.1103/PhysRev.140.A1133, 1965.
[33] P. Giannozzi, S. Baroni, N. Bonini, M. Calandra, R. Car, C. Cavazzoni, D. Ceresoli, G.L. Chiarotti, M. Cococcioni, I. Dabo, A. Dal Corso, S. Fabris, G. Fratesi, S. de Gironcoli, R. Gebauer, U. Gerstmann, C. Gougoussis, A. Kokalj, M. Lazzeri, L. Martin-Samos, N. Marzari, F. Mauri, R. Mazzarello, S. Paolini, A. Pasquarello, L. Paulatto, C. Sbraccia, S. Scandolo, G. Sclauzero, A.P. Seitsonen, A. Smogunov, P. Umari, R.M. Wentzcovitch, QUANTUM ESPRESSO: a modular and open-source software project for quantum simulations of materials, J. Phys.: Condens. Matter 21 (2009) 395502, https://doi.org/10.1088/0953-8984/21/39/395502.
[34] https://www.quantumespresso.org (last accessed on 17th January 2025).
[35] P.E. Blöchl, Projector augmented-wave method, Phys. Rev. B 50 (1994) 17953, https://doi.org/10.1103/PhysRevB.50.17953.
[36] We used the pseudopotentials H.pbe-kjpaw_psl.1.0.0.UPF, B.pbe-n-kjpaw_psl.1.0.0.UPF, C.pbe-n-kjpaw_psl.1.0.0.UPF, and O.pbe-n-kjpaw_psl.1.0.0.UPF, from, https://pseudopotentials.quantum-espresso.org/legacy_tables, 2024. last accessed on 27th November.
[37] J.P. Perdew, K. Burke, M. Ernzerhof, Generalized gradient approximation made simple, Phys. Rev. Lett. 77 (1996) 3865–3868, https://doi.org/10.1103/PhysRevLett.77.3865.
[38] S. Grimme, J. Antony, S. Ehrlich, H. Krieg, A consistent and accurate ab initio parametrization of density functional dispersion correction (DFT-D) for the 94 elements H-Pu, J. Chem. Phys. 132 (2010) 154104, https://doi.org/10.1063/1.3382344.
[39] H.J. Monkhorst, J.D. Pack, Special points for Brillouin-zone integrations, Phys. Rev. B 13 (1976) 5188, https://doi.org/10.1103/PhysRevB.13.5188.
[40] A. Seif, M.J. López, A. Granja-DelRío, K. Azizi, J.A. Alonso, Adsorption and growth of palladium clusters on graphdiyne, Phys. Chem. Chem. Phys. 19 (2017) 19094–19102, https://doi.org/10.1039/c7cp03263c.
[41] H.C. Andersen, Molecular dynamics simulations at constant pressure and/or temperature, J. Chem. Phys. 72 (1980) 2384–2393, https://doi.org/10.1063/1.439486.
[42] N. Mehio, S. Dai, D. Jiang, Quantum mechanical basis for kinetic diameters of small gaseous molecules, J. Phys. Chem. A 118 (2014) 1150–1154, https://doi.org/10.1021/jp412588f.
[43] J. Guo, G. Galliero, R. Vermorel, From molecular sieving to gas effusion through nanoporous 2D graphenes: comparison between analytical predictions and molecular simulations, J. Chem. Phys. 159 (2023) 084701, https://doi.org/10.1063/5.0161980.
[44] Juncheng Guo, G. Galliero, R. Vermorel, How membrane flexibility impacts permeation and separation of gas through nanoporous graphenes, Nano Lett. 24 (2024) 12292–12298, https://doi.org/10.1021/acs.nanolett.4c03580.
[45] W.P. Wang, R.G. Parr, Statistical atomic models with piecewise exponentially decaying electron densities, Phys. Rev. A 16 (1977) 891–902, https://doi.org/10.1103/PhysRevA.16.891.
[46] N.A. Cordero, N.H. March, J.A. Alonso, Ionization potentials of neutral atoms and positive ions in the limit of large atomic number, Phys. Rev. A 75 (2007) 012505, https://doi.org/10.1103/PhysRevA.75.012505.
[47] B. Xu, H. Xiang, Q. Wei, J.Q. Liu, Y.D. Xia, J. Yin, Z.G. Liu, Two-dimensional graphene-like C_2N: an experimentally available porous membrane for hydrogen purification, Phys. Chem. Chem. Phys. 17 (2015) 15115–15118, https://doi.org/10.1039/c5cp01789k.
[48] Z. Yuan, A.G. Rajan, R.P. Misra, L.W. Drahushuk, K.V. Agrawal, M.S. Strano, D. Blankschtein, Mechanism and prediction of gas permeation through sub-nanometer graphene pores: comparison of heory and simulation, ACS Nano 11 (2017) 7974–7987, https://doi.org/10.1021/acsnano.7b02523.
[49] Z. Yuan, R.P. Misra, A.G. Rajan, M.S. Strano, D. Blankschtein, Analytical prediction of gas permeation through graphene nanopores of varying sizes: understanding transitions across multiple transport regimes, ACS Nano 13 (2019) 11809–11824, https://doi.org/10.1021/acsnano.9b05779.